



Free vibration analysis of a functionally graded material beam: evaluation of the Haar wavelet method

Maarjus Kirs^{a*}, Kristo Karjust^a, Imran Aziz^b, Erko Õunapuu^a, and Ernst Tungal^a

^a Department of Mechanical and Industrial Engineering, School of Engineering, Tallinn University of Technology, Ehitajate tee 5, 19086 Tallinn, Estonia

^b Department of Mathematics, University of Peshawar, Peshawar, Pakistan

Received 1 December 2016, revised 14 March 2017, accepted 10 May 2017, available online 17 August 2017

© 2018 Authors. This is an Open Access article distributed under the terms and conditions of the Creative Commons Attribution-NonCommercial 4.0 International License (<http://creativecommons.org/licenses/by-nc/4.0/>).

Abstract. The current study focuses on the evaluation of the Haar wavelet method, i.e. its comparison with widely used strong formulation based methods (FDM-finite difference method and DQM-differential quadrature method). A solid element 3D finite element model is developed and the numerical results obtained by using simplified approaches are confirmed.

Key words: Haar wavelet method, convergence, accuracy evaluation.

1. INTRODUCTION

Accuracy and complexity are two key factors characterizing any numerical method. The Haar wavelet method (HWM) considered in the current study was introduced by Chen and Hsiao in [1,2] almost 20 years ago and up to now it has been applied for solving a wide class of differential and integral equations covering engineering, economic, etc. problems [3–7]. An overview of the applications of the HWM is given in [8]. The wavelet techniques based on the use of an operational matrix of integration are developed for solving ordinal and partial differential equations in [1–10] and for integral equations in [11–13]. All these studies implement the strong formulation based approach of the HWM. The weak formulation based approach of the HWM was introduced in [14].

Most of the authors characterize the HWM as a simple and effective method [3–9]. These estimates cover mainly implementation of the HWM, less its

accuracy and convergence results, which are still under development. It is shown in [15] that in the case of function approximation with direct expansion into the Haar wavelet the convergence is of order one. However, according to the HWM approach considered, the highest order derivative included in the differential equation is expanded into a series of Haar functions. Thus, the estimate given in [15] holds good for estimating the accuracy of the highest order derivative, but not the solution of the differential equation. Recently, the convergence theorem of the HWM was proved in [16] for the n th order ordinal differential equations (ODEs) ($n \geq 2$). It was stated that the order of convergence of the HWM is equal to two. In [17] the accuracy estimates for the extrapolated results in the case of the fourth order ODE are derived, and it is shown that the order of convergence of the extrapolated results is equal to four (Richardson extrapolation is applied).

The application area of new simple methods often includes problems with advanced material models, constitutive laws, etc., which are not yet (well) covered by commercial software.

* Corresponding author, Maarjus.Kirs@ttu.ee

A new trend in the development of wavelet methods can be outlined as solution of fractional differential and integral equations [15,18–24], which is an area not yet well covered by commercial software (finite element method (FEM), etc.). It is observed in [21] that in the case of fractional ODE the order of convergence of the HWM is equal to two if higher order derivative α in the fractional differential equation exceeds one ($\alpha > 1$). However, in the case of $0 < \alpha < 1$ the order of convergence of the HWM tends to the value $1 + \alpha$.

In [25,26] the HWM was adapted for the analysis of structures of functionally graded material (FGM). In the current study the vibration analysis of the FGM beams is performed and the results obtained by the HWM are compared with the corresponding results obtained by using the finite difference method (FDM) and the differential quadrature method (DQM). Selection of FDM and DQM for comparison of results was motivated by the fact that these methods are widely used numerical methods in engineering and are based on strong formulation (the complexity of implementation is similar). The methods considered are implemented by the authors in the MATLAB code.

In order to verify the obtained results and prepare solution procedures for structures with complex geometry and loading cases, the solid element 3D finite element model was developed.

2. BASICS OF HAAR WAVELETS

The Haar function is defined in [8,9] as

$$h_i(x) = \begin{cases} 1 & \text{for } x \in [\xi_1(i), \xi_2(i)] \\ -1 & \text{for } x \in [\xi_2(i), \xi_3(i)] \\ 0 & \text{elsewhere} \end{cases} \quad (1)$$

In (1) $i = m + k + 1$, $m = 2^j$ is the maximum number of square waves that can be sequentially deployed in interval $[A, B]$ and the parameter k indicates the location of the particular square wave,

$$\begin{aligned} \xi_1(i) &= A + 2k\mu\Delta x, \\ \xi_2(i) &= A + (2k+1)\mu\Delta x, \\ \xi_3(i) &= A + 2(k+1)\mu\Delta x, \\ \mu &= M/m, \Delta x = (B-A)/(2M), M = 2^j. \end{aligned} \quad (2)$$

The Haar functions are orthogonal to one another and form a good transform basis

$$\int_0^1 h_i(x)h_l(x)dx = \begin{cases} 2^{-j} & i=l=2^j+k \\ 0 & i \neq l \end{cases} \quad (3)$$

Any function $f(x)$ that is square integrable and finite in the interval $[A, B]$ can be expanded into Haar wavelets as

$$f(x) = \sum_{i=1}^{\infty} a_i h_i(x). \quad (4)$$

The integrals of the Haar functions (1) of order n can be calculated analytically as [9]

$$p_{n,i}(x) = \begin{cases} 0 & x \in [A, \xi_1(i)] \\ \frac{(x-\xi_1(i))^n}{n!} & x \in [\xi_1(i), \xi_2(i)] \\ \frac{(x-\xi_1(i))^n - 2(x-\xi_2(i))^n}{n!} & x \in [\xi_2(i), \xi_3(i)] \\ \frac{(x-\xi_1(i))^n - 2(x-\xi_2(i))^n + (x-\xi_3(i))^n}{n!} & x \in [\xi_3(i), B] \end{cases} \quad (5)$$

The integrals of the Haar functions determined by (5) are continuous functions in the interval $[A, B]$.

3. FREE VIBRATION ANALYSIS OF THE FGM BEAM

In the following the free vibration analysis of the FGM beam is considered [27–29]. It is assumed that the material properties of the beam of length L vary axially. The governing differential equation of the beam can be written as

$$\frac{\partial^2}{\partial x^2} \left(EI(x) \frac{\partial^2 w(x,t)}{\partial x^2} \right) + \rho A(x) \frac{\partial^2 w(x,t)}{\partial t^2} = 0, \quad (6)$$

$$0 < x < L.$$

The varying properties of the bending stiffness $EI(x)$ and the distributed mass per unit length $\rho A(x)$ are described by exponential functions as

$$EI(x) = EI(0)e^{2\beta x/L}, \rho A(x) = \rho A(0)e^{2\beta x/L}. \quad (7)$$

The reference values of the bending stiffness and distributed mass per unit length at $x = 0$ are denoted by $EI(0)$ and $\rho A(0)$, respectively. Relation (7) is used in a number of papers [27–29]. The volume fractions of the material corresponding to relation (7) can be derived as

$$V_1 = \frac{e^{2\beta} - e^{2\beta x}}{e^{2\beta} - 1}, \quad V_2 = \frac{e^{2\beta x} - 1}{e^{2\beta} - 1}. \quad (8)$$

The wavelet method approach considered can be applied for a wide range of functions describing

properties of FGM. In the following a more general power law relation for describing FG materials is considered:

$$E = (E_L - E_R) \left(1 - \frac{x}{L}\right)^k + E_R, \quad (9)$$

$$\rho = (\rho_L - \rho_R) \left(1 - \frac{x}{L}\right)^k + \rho_R. \quad (10)$$

Here k is the non-negative power-law exponent describing the material variation profile along the length of the beam and the indexes L and R stand for the values of the material properties on the left and right support of the beam, respectively. Relations (9)–(10) seem to be the most widely used relations for describing FGM properties found in the literature [30].

In the following the solution of the partial differential equation (6) is assumed in the form

$$w(x, t) = W(x) \sin(\omega t). \quad (11)$$

Considering Eqs (7) and (11), the governing differential equation (6) can be rewritten in a non-dimensional form as

$$\frac{d^2}{dx^2} \left(e^{2\beta x} \frac{d^2 W}{dx^2} \right) - \Omega^2 e^{2\beta x} W = 0, \quad (12)$$

where

$$X = \frac{x}{L}, \Omega = 2\pi fL^2 \sqrt{\frac{\rho A(0)}{EI(0)}}. \quad (13)$$

As a result, the vibration analysis problem of the FGM beam considered above is converted to solving the ordinal differential equation (12). The particular boundary conditions are introduced in Section 7.

4. THE HAAR WAVELET DISCRETIZATION METHOD

Herein the most commonly used approach of the HWM is employed. According to this method, the highest order derivative existing in a differential equation is expanded into Haar wavelets. Thus, Eq. (12) implies that the fourth order derivative should be expanded into Haar wavelets as

$$\frac{d^4 W}{dX^4} = \sum_{i=1}^N a_i h_i(X), \quad (14)$$

where $N = 2M$ is the resolution used.

The solution of the differential governing equation (12) $W(X)$ can be obtained by integrating the expansion (14) four times with respect to X as

$$W(X) = a^T P^{(4)} + c_3 \frac{X^3}{6} + c_2 \frac{X^2}{2} + c_1 X + c_0. \quad (15)$$

In (15) the operational matrix of integration $P^{(4)}$ is defined by formulas (5) and a^T is a vector of coefficients. The integration constants c_0, \dots, c_3 can be determined for each particular boundary condition separately. Corresponding expressions of the integration constants are omitted for conciseness sake.

Inserting the solution of (15) in the differential equation (12) and assuming uniform grid points in the form

$$t_l = (2l - 1)/(2N), \quad l = 1, \dots, N, \quad (16)$$

one obtains a linear system of algebraic equations, which can be solved with respect to coefficient vector a^T . Finally, substituting the values of a^T in (15) gives the solution of the posed problem in an analytical form.

5. CONVERGENCE AND ACCURACY ESTIMATES

The convergence theorem for the HWM is given in [16] for the n th order ODE ($n \geq 2$) as

THEOREM: Let us assume that $f(x) = \frac{d^n u(x)}{dx^n} \in L^2(R)$

is a continuous function on $[0, 1]$ and its first derivative is bounded

$$\forall x \in [0, 1] \exists \eta : \left| \frac{df(x)}{dx} \right| \leq \eta. \quad (17)$$

Then the HWM, based on the approach in [1, 2], will be convergent, i.e. $|E_M|$ will vanish as the number of collocation points approaches N infinity. The convergence is of the order two

$$\|E_M\|_2 = O \left[\left(\frac{1}{N} \right)^2 \right]. \quad (18)$$

The proof of the theorem is given in [16]. Furthermore, the quadrate of the L^2 -norm of the error function can be estimated as

$$\|E_M\|_2 \leq \frac{4}{9} \frac{\eta}{(\text{floor}(n/2)!)^2} \left(\frac{1}{N} \right)^2. \quad (19)$$

In the case of the considered problem the highest order derivative in differential equation equals four ($n = 4$) and formula (19) reduces to

$$\|E_M\|_2 \leq \frac{\eta}{9} \left(\frac{1}{N}\right)^2. \quad (20)$$

Furthermore, it is proved in [17] that in the case of the general fourth-order ODE the accuracy of the results of the HWM can be improved from two to four by applying Richardson's extrapolation method. The theoretical estimates pointed out above are validated numerically in the following section.

6. FEM SIMULATION MODEL

Commercial analysis software Mechanical APDL 16.0 was used to develop a 3D finite element simulation model for free vibration analysis of an axially functionally graded beam. The FGM beam was partitioned through its length into a number of strips with constant material properties inside the strip (see Fig. 1).

Figure 1 shows the mesh of the zoomed right-hand side of the beam corresponding to the third row of Table 1 (5 elements in the thickness and width directions and 500 elements in the length direction). The elements considered were cubical 3D 8-Node Homogeneous Structural Elements SOLID185. The detailed mesh values used are given in column 1 of Table 1.

The geometrical parameters of the beam considered are width (b), height (h), and length (L). The material properties of the steel and aluminium used in the FEM analysis are given in Table 2. The boundary conditions considered correspond to a cantilever beam. The results obtained from FEM analysis were originally in the

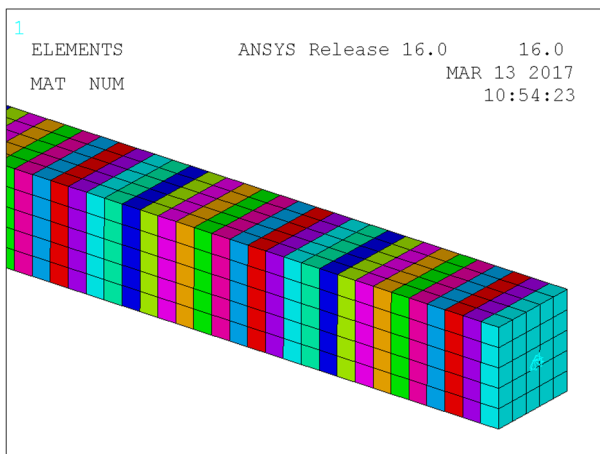


Fig. 1. FGM beam. Mesh, zoomed right end of the beam.

Table 1. FEM model. First three values of frequency parameter, pinned–pinned beam

N	Ω_1	Ω_2	Ω_3
2700 ($3 \times 3 \times 300$)	8.4522	41.2579	91.5302
6400 ($4 \times 4 \times 400$)	8.4366	41.1807	91.3549
12500 ($5 \times 5 \times 500$)	8.4276	41.1363	91.2543
100000 ($10 \times 10 \times 1000$)	8.4136	41.0672	91.0984

Table 2. Material properties of FG steel/aluminium material

Property	Unit	Steel	Aluminium
E	GPa	210	70
ρ	Kg/m ³	7800	2600

dimensional form, i.e. computed for a particular beam with the given geometry, rigidity, and mass per unit length values. In order to compare these results with the results of the FDM, DQM, and HWM, the frequency parameter was converted into the non-dimensional form using the following formula:

$$\Omega = 2\pi fL^2 \sqrt{\frac{\rho A(0)}{EI(0)}}, \quad (21)$$

where f stands for natural/dimensional frequency parameter value (in Hz). The FEM results are discussed in detail in the following section.

7. NUMERICAL RESULTS

In the following five different boundary conditions of the FGM beam are considered (see Fig. 2) and the results obtained by applying HWM, FDM, and DQM are compared (two symmetric and three non-symmetric conditions).

The first two values of the fundamental frequency parameter Ω are presented in Tables 3 and 4 for a pinned–pinned beam, in Tables 5 and 6 for a clamped–clamped beam, in Tables 7 and 8 for a clamped–pinned beam, in Tables 9 and 10 for a pinned–clamped beam, and in Tables 11 and 12 for a clamped–free beam).

Note that in the FE model all supports with pinned boundary conditions (a, c, and d) have the ability to move in the horizontal direction ($u_y = u_z = 0, u_x \neq 0$).

In Tables 1–10 the properties of the beam are considered to vary according to formula (7), i.e. by exponential functions.

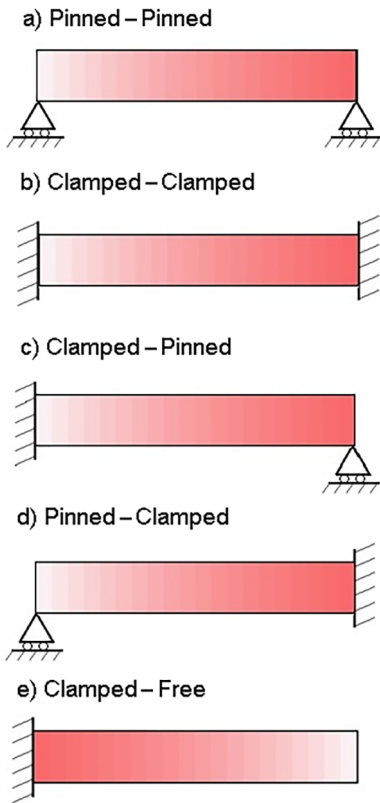


Fig. 2. Boundary conditions of the FGM beam.

Table 3. Fundamental frequency parameter Ω_1 ($\beta = 2$, exact solution 8.41047573)

N	HWM	FDM	DQM
4	7.235577	8.157141	
8	8.118951	8.332735	8.40822662
16	8.337942	8.390010	8.41047574
32	8.392365	8.405292	8.41047574
64	8.405950	8.409176	8.41047568
128	8.409344	8.410150	8.41047711
256	8.410193	8.410394	8.41047514
FEM results ($10 \times 10 \times 1000$ el.)			8.4136

Table 4. Second natural frequency parameter Ω_2 ($\beta = 2$, exact solution 41.07055822)

N	HWM	FDM	DQM
4	36.595239	34.453858	
8	39.999094	39.252370	41.07596761
16	40.805039	40.603112	41.07055821
32	41.004320	40.952833	41.07055821
64	41.054008	41.041072	41.07055830
128	41.066421	41.063183	41.07055855
256	41.069524	41.068714	41.07056029
FEM results ($10 \times 10 \times 1000$ el.)			41.0672

Table 5. Fundamental frequency parameter Ω_1 ($\beta = 2$, exact solution 24.78955023)

N	HWM	FDM	DQM
4	21.242723	21.212781	
8	24.016796	23.517337	24.24277247
16	24.602325	24.432036	24.78954915
32	24.743104	24.697286	24.78955023
64	24.777961	24.766296	24.78955023
128	24.786654	24.783725	24.78955013
256	24.788826	24.788093	24.78955092
FEM results ($10 \times 10 \times 1000$ el.)			24.8074

Table 6. Second natural frequency parameter Ω_2 ($\beta = 2$, exact solution 64.70943426)

N	HWM	FDM	DQM
4	57.202697		
8	62.966887	57.405312	65.21032574
16	64.287324	62.612504	64.70946202
32	64.604874	64.163748	64.70943427
64	64.683357	64.571582	64.70943427
128	64.702919	64.674880	64.70943434
256	64.707806	64.700790	64.70943804
FEM results ($10 \times 10 \times 1000$ el.)			64.7032

Table 7. Fundamental frequency parameter Ω_1 ($\beta = 2$, exact solution 11.18278324)

N	HWM	FDM	DQM
4	8.764599	9.455451	
8	10.647800	10.572089	11.17258124
16	11.052596	11.012971	11.18278324
32	11.150448	11.139111	11.18278324
64	11.174712	11.171786	11.18278327
128	11.180766	11.180029	11.18278302
256	11.182279	11.182094	11.18278285
FEM results ($10 \times 10 \times 1000$ el.)			11.1901

Table 8. Second natural frequency parameter Ω_2 ($\beta = 2$, exact solution 48.26066843)

N	HWM	FDM	DQM
4	41.945882	35.930268	
8	46.799191	43.888087	48.31401606
16	47.903565	47.016589	48.26066840
32	48.171942	47.938093	48.26066844
64	48.238522	48.179262	48.26066848
128	48.255134	48.240268	48.26066852
256	48.259285	48.255565	48.26066842
FEM results ($10 \times 10 \times 1000$ el.)			48.2589

Table 9. Fundamental frequency parameter Ω_1 ($\beta = 2$, exact solution 20.777978)

N	HWM	FDM	DQM
4	18.799637	19.770973	
8	20.309972	20.506995	20.77852832
16	20.662461	20.708729	20.77797932
32	20.749190	20.760567	20.77797932
64	20.770788	20.773620	20.77797931
128	20.776182	20.776889	20.77797921
256	20.777530	20.777707	20.77797837
FEM results ($10 \times 10 \times 1000$ el.)			20.7897

Table 10. Second natural frequency parameter Ω_2 ($\beta = 2$, exact solution 56.294438)

N	HWM	FDM	DQM
8	54.965168	52.599124	
16	55.969009	55.338806	56.09705480
32	56.213501	56.053355	56.29443879
64	56.274230	56.234028	56.29443858
128	56.289388	56.279327	56.29443857
256	56.293176	56.290660	56.29443848
FEM results ($10 \times 10 \times 1000$ el.)			56.2907

Table 11. Fundamental frequency parameter Ω_1 ($\beta = -0.549306$)

N	HWM	FDM	DQM
8	4.884627	4.842031	4.87118515
16	4.874540	4.863858	4.87119849
32	4.872033	4.869360	4.87119848
64	4.871407	4.870739	4.87119797
128	4.871251	4.871084	4.87120621
256	4.871212	4.871170	4.87220829
FEM results ($10 \times 10 \times 1000$ el.)			4.8758

Table 12. Second natural frequency parameter Ω_2 ($\beta = -0.549306$)

N	HWM	FDM	DQM
8	24.798280	23.143597	24.41704668
16	24.517676	24.092313	24.42645172
32	24.449153	24.342014	24.42645172
64	24.432120	24.405285	24.42645167
128	24.427868	24.421156	24.42645138
256	24.426806	24.425128	24.42665633
FEM results ($10 \times 10 \times 1000$ el.)			24.4397

In Tables 3–10 the value of the parameter β is taken equal to 2. The exact solutions computed based on transcendental algebraic equations derived in [27] are given in the headings of Tables 3–10. Obviously, the convergence of the HWM (also of the FDM and DQM) to the exact solution can be observed in all these tables.

The numerical rates of the convergence, computed for the solutions presented in Table 3, are presented in Table 13.

In Table 13 the values of N start from 16 because each rate of convergence was computed on the basis of three consecutive values of the solution [16]. The rate of the convergence of the HWM and FDM obviously tends to two, but the DQM has an ultrafast rate for $N \leq 32$ and a negative rate for $N > 32$ (loss of accuracy).

In Table 14, the convergence rates of the extrapolated results of the HWM are given for four different boundary conditions considered above. The Richardson extrapolation method was applied, and it can be seen from Table 14 that the order of the convergence of extrapolated results tends to four in the case of all boundary conditions considered.

Based on results given in Tables 3–12, it can be concluded that in the case of the posed problem the highest accuracy was achieved by applying the DQM, also in most cases the accuracy of the results obtained by the HWM is higher than that obtained by the FDM (there fundamental frequencies in Tables 3 and 7 are exceptions). Detailed analysis of DQM results shows that the maximum accuracy was achieved extremely quickly with $N = 16$ or $N = 32$; thereafter the accuracy of the solution decreased with increasing resolution. These results are in agreement with the theoretical concept of the DQM (it is based on the use of high order polynomials whose denominator vanishes for large N) and results found in the literature.

It can be seen from Fig. 3 that in the case of the parameter value $k = 1.5$ the functions of the elasticity modulus corresponding to the exponential and power law functions (7) and (9) are close (here a steel/aluminium cantilever beam with $\beta = -0.549306$ is considered).

Table 13. Rates of convergence corresponding to results given in Table 3

N	HWM	FDM	QDM
16	2.0122	1.6163	–
32	2.0086	1.9060	23.8789
64	2.0023	1.9766	–8.6258
128	2.0006	1.9942	–4.6331
256	2.0001	1.9985	–0.4590

Table 14. Fundamental frequency parameter Ω_1 , convergence rates of extrapolated results

N	Pinned–pinned	Clamped–clamped	Clamped–pinned	Pinned–clamped
32	2.514821	4.2685	4.3015	4.1711
64	3.916921	4.0516	4.0774	4.0425
128	3.984539	4.0120	4.0191	4.0105
256	3.996411	4.0029	4.0047	4.0026

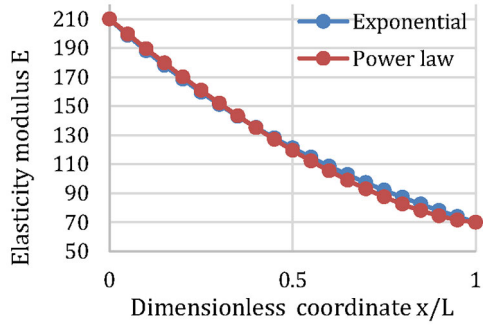


Fig. 3. Variation of elastic modulus.

In Tables 11 and 12 the FG material properties corresponding to steel/aluminium are considered with steel in the left and aluminium in the right support. The particular values of the material used are presented in Table 2.

The exponential model (7) does not include directly material properties at the right end of the beam. The required values of the material are obtained by determining the value of the parameter β ($\beta = -0.549306$).

The first four mode shapes for the above-considered FG steel/aluminium cantilever beam are depicted in Fig. 4. The corresponding mode shapes obtained by a FEM are shown in Figs 5–8.

The results given in Table 15 were obtained by applying the HWM with the general power law function (9)–(10).

The steel/aluminium FGM with properties given in Table 2 is considered and the value of the exponent is taken equal to 1.5 ($k = 1.5$). The boundary conditions for a clamped–clamped beam are applied.

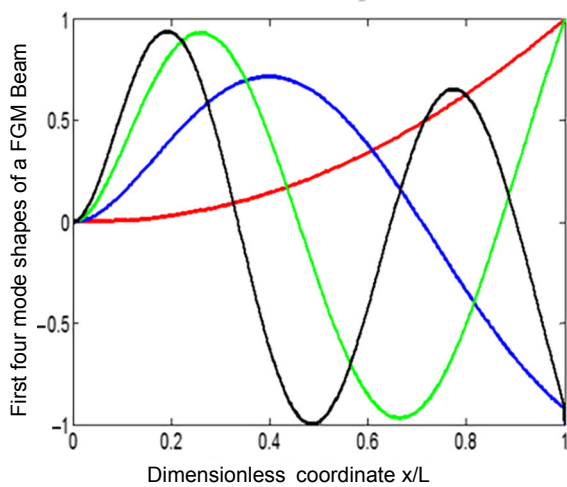


Fig. 4. First four mode shapes of a cantilever FGM beam.

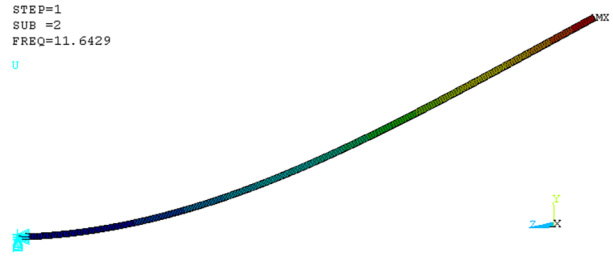


Fig. 5. First mode shape of a cantilever FGM beam in FEM.

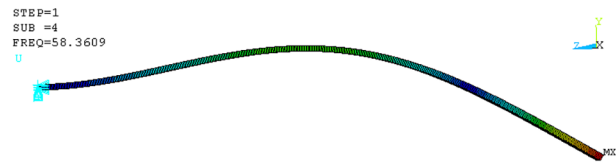


Fig. 6. Second mode shape of a cantilever FGM beam in FEM.

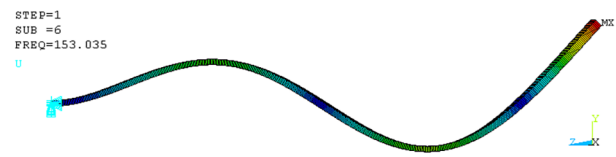


Fig. 7. Third mode shape of a cantilever FGM beam in FEM.

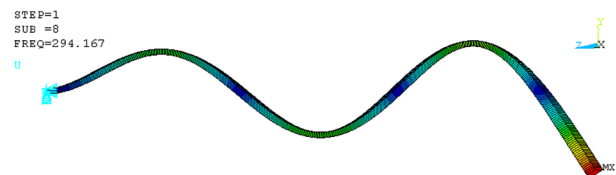


Fig. 8. Fourth mode shape of a cantilever FGM beam in FEM.

Table 15. First three values of fundamental frequency parameter ($k = 1.5$, power law)

N	Ω_1	Ω_2	Ω_3
8	22.573818	62.648322	124.802042
16	22.559805	62.097576	122.045771
32	22.552926	61.958469	121.384345
64	22.548905	61.920592	121.216644
128	22.546296	61.908898	121.172322
256	22.544517	61.904408	121.159519

The FEM results computed for all boundary conditions considered above are given in the last row of each table. The number of elements used is $10 \times 10 \times 1000$.

Obviously, the values of the frequency parameters computed using 3D FEM analysis are in excellent agreement with those given in Tables 3–12, obtained by applying the HWM, DQM, and FDM.

An example of the results of more detailed FEM analysis is given in Table 15. In this table the first free frequencies for a pinned–pinned beam are presented. The convergence of the solution with increasing mesh can be observed. The results are in agreement with corresponding results obtained by applying the HWM, FDM, and DQM given in Tables 3 and 4.

8. CONCLUSIONS

Three strong formulation based numerical methods (HWM, FDM, and DQM) were applied for the analysis of the FGM beam and the obtained results were compared. The algorithms for all methods were coded by the authors in MATLAB. Good performance was observed in the case of all three methods used.

It can be concluded that in the case of the considered problem the accuracy of the solutions obtained by applying the HWM and FDM was in the same range. However, in most cases the accuracy of the results of the HWM outperformed that of the FDM. The accuracy of the DQM appears to be higher than that of the HWM and FDM. The convergence results presented in Table 13 confirm the accuracy of the HWM, FDM, and DQM. Similar accuracy was observed also for cylindrical shells in [16].

The obtained numerical results were validated with the solid element 3D finite element model developed for analysing more complex FGM structures. The results obtained with applying the 3D FEM and HWM were found to be in good (rather excellent) agreement.

Our future studies will focus on the application of the HWM for the analysis of nanostructures and solving fractional differential equations, which are not yet well covered by commercial software solutions. An interesting subtopic, whose research is underway, is adaption of global optimization methods and techniques, developed by the workgroup of design composite structures [31–36] to design nano- and graphene structures.

ACKNOWLEDGEMENTS

The research was supported by the Estonian Research Council (grant PUT1300); Estonian Centre of Excellence in Zero Energy and Resource Efficient Smart Buildings and Districts, ZEBE, TK146 funded by the European Regional Development Fund (grant 2014-2020.4.01.15-0016); Innovative Manufacturing Engineering Systems

Competence Centre IMECC (supported by Enterprise Estonia and co-financed by the European Union Regional Development Fund, project EU48685). The publication costs of this article were covered by Tallinn University of Technology and the Estonian Academy of Sciences.

REFERENCES

- Chen, C. F. and Hsiao, C. H. Haar wavelet method for solving lumped and distributed-parameter systems. *IEE Proc. Contr. Theor. Appl.*, 1997, **144**(1), 87–94.
- Hsiao, C. H. State analysis of the linear time delayed systems via Haar wavelets. *Math. Comp. Simulat.*, 1997, **44**(5), 457–470.
- Majak, J., Pohlak, M., and Eerme, M. Application of the Haar wavelet problems of orthotropic plates and shells. *Mechanic of Composite Materials*, 2009, **45**(6), 631–642.
- Kirs, M., Mikola, M., Haavajõe, A., Öunapuu, E., Shvartsman, B., and Majak, J. Haar wavelet method for vibration analysis of nanobeams. *Waves, Wavelets and Fractals – Advanced Analysis*, 2016, **2**, 20–28.
- Lepik, Ü. Solving PDEs with the aid of two dimensional Haar wavelets. *Comput. Math. Appl.*, 2011, **61**, 1873–1879.
- Lepik, Ü. Solving fractional integral equations by the Haar wavelet method. *Appl. Math. Comput.*, 2009, **214**(2), 468–478.
- Xie, X., Jin, G., Yan, Y., Shi, S. X., and Liu, Z. Free vibration analysis of composite laminated cylindrical shells using the Haar wavelet method. *Compos. Struct.*, 2014, **109**, 169–177.
- Lepik, Ü. Numerical solution of differential equations using Haar wavelets. *Math. Comput. Simulat.*, 2005, **68**, 127–143.
- Lepik, Ü. and Hein, H. *Haar Wavelets: With Applications*. Springer, New York, 2014.
- Ray, S. S. and Patra, A. Numerical simulation based on Haar wavelet operational method to solve neutron point kinetics equation involving sinusoidal and pulse reactivity. *Ann. Nucl. Energy*, 2014, **73**, 408–412.
- Islam, S. U., Aziz, I., and Al-Fhaid, A. S. An improved method based on Haar wavelets for numerical solution of nonlinear integral and integro-differential equations of first and higher orders. *J. Comput. Appl. Math.*, 2014, **260**, 449–469.
- Aziz, I., Islam, S. U., and Khana, F. A new method based on Haar wavelet for the numerical solution of two-dimensional nonlinear integral equations. *J. Comput. Appl. Math.*, 2014, **272**, 70–80.
- Aziz, I. and Islam, S. U. New algorithms for the numerical solution of nonlinear Fredholm and Volterra integral equations using Haar wavelets. *J. Comput. Appl. Math.*, 2013, **239**, 333–345.
- Majak, J., Pohlak, M., Eerme, M., and Lepikult, T. Weak formulation based Haar wavelet method for solving differential equations. *Appl. Math. Comput.*, 2009, **211**(2), 488–494.
- Saeedi, H., Mollahasani, N., Moghadam, M., and Chuev, G. An operational Haar wavelet method for solving fractional Volterra integral equations. *Int. J. Appl. Math. Comput. Sci.*, 2011, **21**(3), 535–547.

16. Majak, J., Shvartsman, B. S., Kirs, M., Pohlak, M., and Herranen, H. Convergence theorem for the Haar wavelet based discretization method. *Compos. Struct.*, 2015, **126**, 227–232.
17. Majak, J., Shvartsman, B. S., Karjust, K., Mikola, M., Haavajõe, A., and Pohlak, M. *Composites. Part B: Engineering*, 2015, **80**, 321–327.
18. Heydari, M. H., Hooshmandasl, M. R., and Mohammadi, F. Legendre wavelets method for solving fractional partial differential equations with Dirichlet boundary conditions. *Appl. Math. Comput.*, 2014, **234**, 267–276.
19. Heydari, M. H., Hooshmandasl, M. R., and Mohammadi, F. Two-dimensional Legendre wavelets for solving time-fractional telegraph equation. *Adv. Appl. Math. Mech.*, 2014, **6**(2), 247–260.
20. Heydari, M. H., Hooshmandasl, M. R., and Ghaini, F. M. M. A new approach of the Chebyshev wavelets method for partial differential equations with boundary conditions of the telegraph type. *Appl. Math. Model.*, 2014, **38**(5–6), 1597–1606.
21. Majak, J., Shvartsman, B., Pohlak, M., Karjust, K., Eerme, M., and Tungel, E. 2016. Solution of fractional order differential equation by the Haar wavelet method. Numerical convergence analysis for most commonly used approach. In *AIP Conference Proceedings*, **1738** (Simos, T., ed.), 480110. <http://dx.doi.org/10.1063/1.4952346> (accessed 2016-11-30).
22. Rehman, M. U. and Khan, R. A. Numerical solutions to initial and boundary value problems for linear fractional partial differential equations. *Appl. Math. Model.*, 2013, **37**, 5233–5244.
23. Ray, S. S. and Patra, A. Haar wavelet operational methods for the numerical solutions of fractional order nonlinear oscillatory Van der Pol system. *Appl. Math. Comput.*, 2013, **220**, 659–667.
24. Saeed, U., Rejman, M., and Iqbal, M. A. Haar wavelet-Picard technique for fractional order nonlinear initial and boundary value problems. *Sci. Res. Essays*, 2014, **9**(12), 571–580.
25. Hein, H. and Feklistova, L. Computationally efficient delamination detection in composite beams using Haar wavelets. *Mech. Syst. Signal Pr.*, 2011, **25**, 2257–2270.
26. Jin, G., Xie, X., and Liu, Z. The Haar wavelet method for free vibration analysis of functionally graded cylindrical shells based on the shear deformation theory. *Compos. Struct.*, 2014, **108**, 435–448.
27. Li, X. F., Kang, Y. A., and Wu, J. X. Exact frequency equations of free vibration of exponentially functionally graded beams. *Appl. Acoust.*, 2013, **74**, 413–420.
28. Lu, Z. R., Lin, X. X., Chen, Y. M., and Huang, M. Hybrid sensitivity matrix for damage identification in axially functionally graded beams. *Appl. Math. Model.*, 2017, **41**, 604–617.
29. Shvartsman, B. and Majak, J. Numerical method for stability analysis of functionally graded beams on elastic foundation. *Appl. Math. Model.*, 2016, **40**, 3713–3719.
30. Alshorbagy, A. E., Eltahir, M. A., and Mahmoud, F. F. Free vibration characteristics of a functionally graded beam by finite element method. *Appl. Math. Model.*, 2011, **35**, 412–425.
31. Aruniit, A., Kers, J., Goljandin, D., Saarna, M., Tall, K., Majak, J., and Herranen, H. Particulate filled composite plastic materials from recycled glass fibre reinforced plastics. *Materials Science (Medžiagotyra)*, 2011, **17**(3), 276–281.
32. Lellep, J. and Majak, J. On optimal orientation of nonlinear elastic orthotropic materials. *Struct. Optimization*, 1997, **14**, 116–120.
33. Majak, J. and Hannus, S. Orientational design of anisotropic materials using the Hill and Tsai-Wu strength criteria. *Mech. Compos. Mater.*, 2003, **39**(6), 509–520.
34. Aruniit, A., Kers, J., Majak, J., Krumme, A., and Tall, K. Influence of hollow glass microspheres on the mechanical and physical properties and cost of particle reinforced polymer composites. *Proc. Estonian Acad. Sci.*, 2012, **61**, 160–165.
35. Herranen, H., Allikas, G., Eerme, M., Vene, K., Otto, T., Gregor, A., et al. Visualization of strain distribution around the edges of a rectangular foreign object inside the woven carbon fibre specimen. *Estonian J. Eng.*, 2012, **18**, 279–287.
36. Pohlak, M., Majak, J., and Eerme, M. 2008. Optimization of car frontal protection systems. In *Proceedings of the 6th international conference of DAAAM Baltic Industrial Engineering, 24–26th April 2008* (Küttner, R. ed.), 123–128.

Funktsionaalgradientmaterjalist tala vabavõnkumised: Haari lainikute meetodi evalveerimine

Maarjus Kirs, Kristo Karjust, Imran Aziz, Erko Õunapuu ja Ernst Tungel

Uurimistöös on keskendunud Haari lainikute meetodi evalveerimisele. Haari lainikute meetodi abil saadud tulemusi on võrreldud insenerirakendustes laialdaselt kasutatavate tugeval formulatsioonil põhinevate meetodite, nagu lõplike vahede meetodi ja diferentsiaalkvadratuuride meetodi tulemustega. Vaadeldava ülesande korral on Haari lainikute meetod lõplike vahede meetodist täpsem. Diferentsiaalkvadratuuride meetod osutus väiksema kollokatsioonipunktide arvu korral Haari lainikute meetodist täpsemaks, kuid selle rakendamine suurema kollokatsioonipunktide arvu korral on komplitseeritud. Samuti on loodud 3D lõplike elementide meetodil põhinev mudel ja selle rakendamisel saadud tulemused on eeltoodud meetodite tulemustega kooskõlas. Haari lainikute meetodi abil saadud lahendi ja ekstra- poleeritud tulemuste koonduvuskiirus on kooskõlas vastavate koonduvusteoreemidega tõestatud teoreetiliste tulemustega.